Preprint of paper published as Measurement Science and Technology. 28 (2017) p., 034004.

Atomic force microscope adhesion measurements and atomistic molecular dynamics simulations at different humidities

Jeremias Seppä[1], Bernhard Reischl[2], Hannu Sairanen[1], Virpi Korpelainen[1], Hannu Husu[1,3], Martti Heinonen[1], Paolo Raiteri[2], Andrew L. Rohl[2], Kai Nordlund[4] and Antti Lassila[1]

[1] VTT Technical Research Centre of Finland Ltd, Centre for Metrology MIKES, P.O. Box 1000, FI-02044 VTT, Finland

[2] Curtin Institute for Computation and Department of Chemistry, Curtin University, GPO Box U1987, Perth, WA 6845, Australia

[3] Current affiliation: nLIGHT Finland, Lohja, Finland

[4] Department of Physics, University of Helsinki, P.O. Box 43, FI-00014, Finland.

E-mail: jeremias.seppa@vtt.fi

Abstract:

Due to their operation principle atomic force microscopes are sensitive to all factors affecting the detected force between the probe and the sample. Relative humidity is an important and often neglected - both in experiments and simulations - factor in the interaction force between atomic force microscope (AFM) probe and sample in air. This paper describes the humidity control system designed and built for the interferometrically traceable metrology AFM (IT-MAFM) at VTT MIKES. The humidity control is based on circulating the air of the AFM enclosure via dryer and humidifier paths with adjustable flow and mixing ratio of dry and humid air. The design humidity range of the system is 20 – 60 %rh. Force-distance adhesion studies at humidity levels between 25 %rh and 53 %rh are presented and compared to an atomistic molecular dynamics simulation. The uncertainty level of the thermal noise method implementation used for force constant calibration of the AFM cantilevers is 10 %, being the dominant uncertainty component of the interaction force measurement uncertainty. Comparing the simulation and the experiment, the primary uncertainties are related to the nominally 7 nm radius and shape of measurement probe apex, possible wear and contamination, and the atomistic simulation technique details. The interaction forces are of the same order of magnitude in simulation and measurement (5 nN). An elongation of a few nanometres of the water meniscus between probe tip and sample, before its rupture, is seen in simulation upon retraction of the tip in higher humidity. This behaviour is also supported by the presented experimental measurement data but the data is insufficient to conclusively verify the quantitative meniscus elongation.

Keywords:

Atomic force microscopy, metrology, adhesion, capillary effects, humidity, force measurement

PACS: 07.79.Lh, 06.20.-f, 68.35.Np, 92.60.Jq, 47.55.nb, 34.20.-b

Submitted to: Measurement Science and Technology, Special issue: NanoScale 2016

1. Introduction

Atomic force microscopy (AFM) is a versatile technique, capable of measuring samples in air and other fluids as well as in vacuum. AFM can be used to measure e.g. nanoscale topography, material boundaries, and for elasticity mapping. The interaction between an AFM probe and a sample at ambient air conditions is strongly affected by the ambient air humidity. The interaction is dominated in dry air by electrostatic and Van der Waals forces, while increasing the relative humidity leads to capillary forces becoming dominant,

especially for hydrophilic surfaces [1]. While air humidity can complicate AFM measurements by e.g. condensing a capillary meniscus between probe and sample and thus contributing to the interaction force and changing the apparent sample topography [2], adjusting relative ambient humidity can even be exploited, for example, to get better hydrophilic/hydrophobic material contrast [1] and to manipulate frictional forces [3].

Because of its importance in AFM measurement, the capillary force has been researched in several studies [3-8, and references therein]. The liquid bridge forming between two bodies in proximity, at a certain humidity level, and the capillary force caused by this meniscus, can be described by continuum theories [9]. However, for true nanoscale objects, or nano-structured surfaces, such analytical models fail to take into account the atomistic details of the interactions of both objects as well as the water. Atomistic molecular dynamics simulations using classical interaction potentials have been used extensively to study the properties of bulk liquid water [10], as well as water at hard hydrophilic and hydrophobic surfaces or at the water/air interface [11-13], dynamics of water adsorption on surfaces as a function of relative humidity [14], inter-surface forces caused by liquid bridges [15], the structure and thermodynamics of water in sub-nanometer gaps [16, 17], the mechanical effect of the presence of water layers on nano-indentation [18], or the imaging mechanism of surfaces and their hydration layers by AFM in liquid [19, 20].

As a part of the MechProNO project [21], interaction forces and mechanical properties of nano-objects were experimentally studied with the interferometrically traceable metrology AFM (IT-MAFM) at MIKES [22]. In order to control the humidity in the IT-MAFM enclosure and to better understand and traceably measure the interaction force in the AFM at different humidity levels, a humidity control system was designed and implemented.

In this paper we first present the upgrade of the IT-MAFM to a humidity controllable metrology AFM, including a relatively large humidity controlled enclosure for the instrument. Then, benchmark adhesion measurements on a silicon sample with a platinum coated and an uncoated silicon probe at different relative humidities in the 25 – 50 %rh range are described. Finally, atomistic molecular dynamics (MD) simulations of a similar experiment are presented, and compared to the adhesion measurements, with discussion of the designs and results.

2. Humidity control of the MIKES metrology AFM

The humidity controller developed for IT-MAFM is based on controlling humidity around the whole AFM and not just around the probe and sample, in contrast to designs with more localized humidity control [1, 4]. The IT-AFM and controller are situated in a vibration isolated table in an air conditioned laboratory room with constant air temperature of 20±0.05 °C and humidity of 47±2 %rh [23]. The AFM is placed in an enclosure with enhanced sealing to prevent water vapour exchange with ambient air. To adjust the humidity, the enclosure is connected to a closed air circulation with a humidity controller. Enclosing larger sections of the AFM instrumentation provides e.g. easy access to sample between experiment runs and allows for the study of bulkier samples. In addition to slower steering and slower changes in humidity, however, the larger enclosure exposes parts of electronics, optics and other components to changing humidity, as mentioned by Stukalov et al. [4]. The target range in this design was from 20 %rh to 60 %rh, which was considered suitable for all the components in the enclosure.

2.1 Humidity control

The AFM humidity control applies the well-known principle of controlled mixing of a humidified air with a dried air. By adjusting the rotameters controlling the flow rates, any air humidity between a minimum and a maximum can be achieved. The limits are set by the dryer and humidifier efficiencies, respectively. The same principle is applied in e.g. the pre-saturator of a humidity generator developed for humidity calibrations by Sairanen et al. [24].

In the AFM humidity control air is divided into two lines as shown in figure 1. One of the lines leads to a humidification chamber where air flows over a water surface and is humidified by evaporation. The dew-point temperature of the humidified air increases at maximum up to about 17 °C, depending on the flow rate and the water level in the chamber. In the other line air flows through a silica gel drying unit where a minimum dew-point temperature of about -40 °C is achieved depending on the flow rate and the condition of the desiccant. Therefore, the system operates in the relative humidity range from 0.5 %rh to 80 %rh at the MIKES laboratory temperature of 20.0 °C. An auxiliary hygrometer (Vaisala HMI 31) assembled to the outlet of the humidity control is used to estimate the condition of the silica gel drying unit, and to estimate efficiency of the humidification and to help adjusting the humidity at the AFM. To prevent silica gel particles and other impurities from flowing to the AFM, a 7 µm filter was assembled to the outlet of the humidity controller.

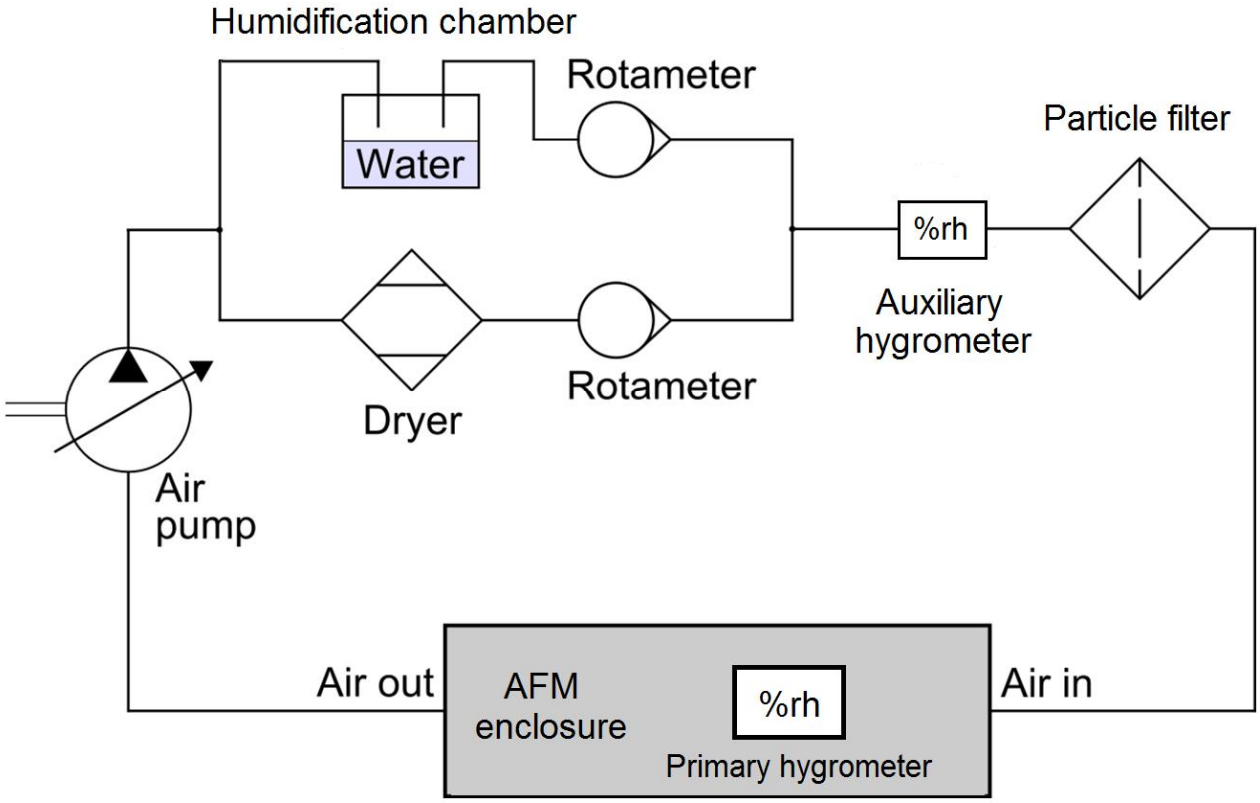

Figure 1. The schema of the AFM humidity controller.

2.2. Humidity controlled AFM enclosure

To enable efficient humidity control in the AFM enclosure, air is pumped in a loop between the enclosure and the flow mixing system. The normal flow rate is about 4 l/min - 5 l/min. Humidity around the AFM head is monitored with a calibrated Vaisala PTU200 hygrometer. This primary humidity sensor is located within approximately 7 cm from the AFM probe and sample. The expanded (k=2) standard uncertainty of the hygrometer calibration in the humidity and temperature range used was less than 1.5 %rh. The inner

dimensions of the AFM enclosure are about 45 cm × 45 cm × 75 cm. Based on measurements, the temperature at the primary humidity sensor differs less than 0.5 °C from the AFM sample stage temperature. This leads to additional 1-2 %rh uncertainty to the humidity at the sample in the cases studied, or less, with smaller temperature gradients.

A key part of the AFM enclosure is a tight sealing. Most of the potential spots of water vapour diffusion are sealed with aluminium tape. Also, components that would slow down the stabilization of humidity are sealed if possible. The input laser beam for the interferometers is guided to the enclosure via an optical glass window. Electrical cables and optical interferometer output fibres are guided via apertures sealed with synthetic rubber foam, aluminium tape and adhesive putty.

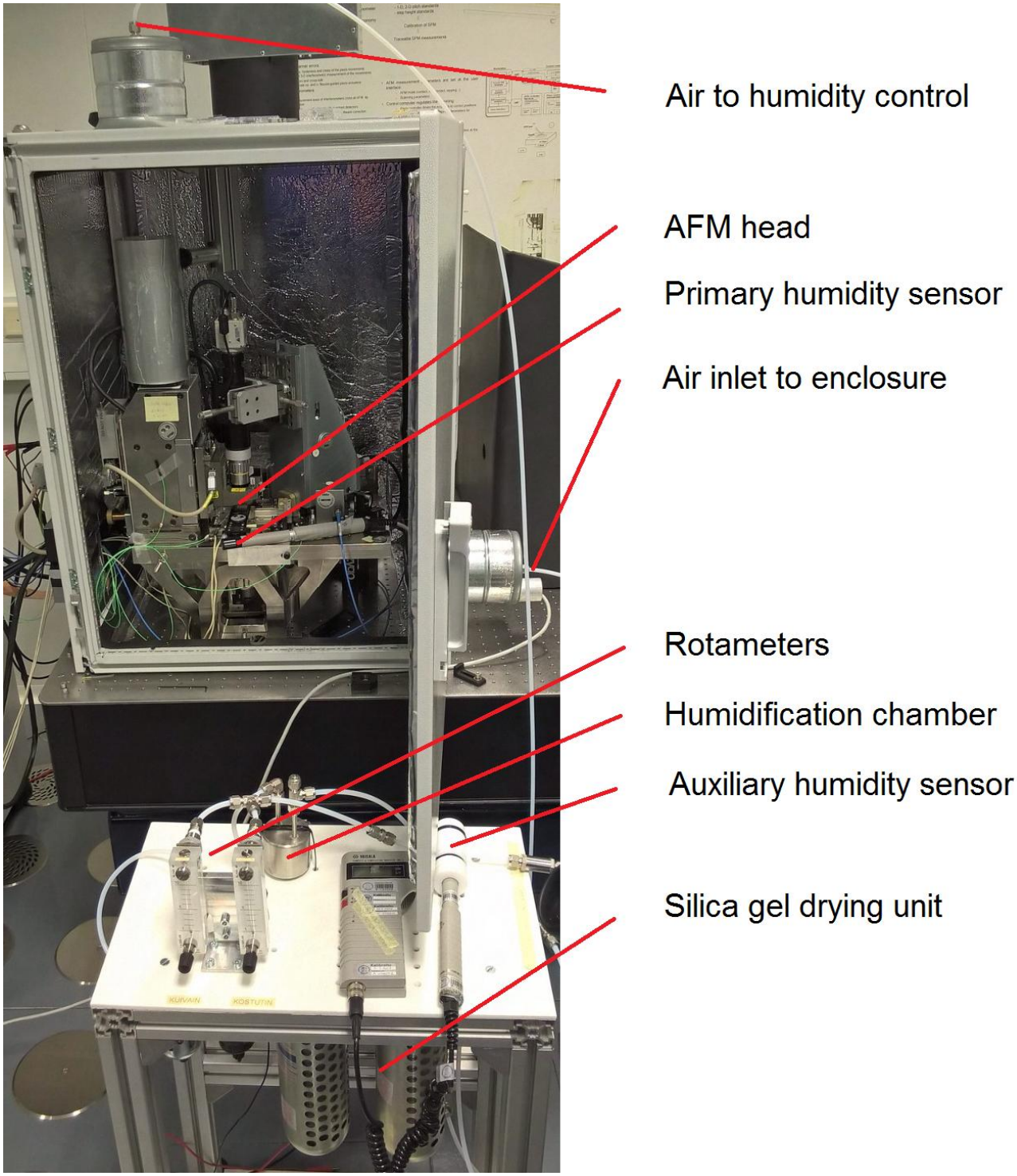

Figure 2. The humidity controlled IT-MAFM enclosure and humidity controller parts shown in the same photograph with annotations.

Due to the extremely low air velocity in the enclosure, slow water vapour diffusion in air and adsorption/desorption on walls, fully stable and homogenous humidity is not feasible. This is naturally also because of residual humidity leaks between laboratory air and enclosure. However, in terms of relative humidity, the largest contributor of inhomogeneity over the whole enclosure are temperature differences, which were also addressed earlier in this subsection. The major heat sources (electronics) are located above and downstream relative to the sites of AFM and humidity measurement, limiting their effects to relative humidity in the measurement sites. The warmer parts of the AFM head tower reach temperatures in the 23-

24 °C range. The achievable relative humidity values are limited at the extremes to a minimum of 20 %rh and maximum of 60 %rh. Figure 3 demonstrates the stabilisation of humidity in the enclosure after supplying air from the dryer to the enclosure originally at the ambient humidity (the ambient relative humidity in the enclosure is also lower than the laboratory air since the enclosure is warmer due to electronics, and in figure 3 the enclosure has been already dried a bit before the start of the recording). In this case the temperature at the sample decreased during experiment from 22.41 to 22.32 °C. The time constant, assessed as the duration when half of the humidity change towards an asymptotic value has happened, seems to be approximately 0.5 hours. During a full range humidity change experiment, the temperature in the AFM enclosure remained stable within 10 mK at 22.28 °C at the measurement site, after warmup of the instrument. An approximately linear drift of the temperature with humidity was observed within the 10 mK range. The AFM noise level with humidity control on at full drying, measured from the Z interferometer signal when measuring a flat sample with 0×0 scan area, is approximately 1.0 nm (rms) or less, depending on sample and AFM control settings.

The air refractive index for interferometry is updated online in the software of the IT-MAFM, based on measured temperatures near the interferometer paths, and the pressure and humidity measured by the primary humidity sensor. The effect of relative humidity on the refractive index is of smaller order of magnitude than the effects of pressure and temperature, which can be seen using e.g. the Edlén equations [25, 26]. For example, a humidity change from 40 to 50 %rh causes only a less than 10^{-7} relative change in refractive index. With the millimetre-level interferometer dead paths (and micrometre-level measured displacements) in the system, this corresponds to an insignificant subnanometre uncertainty contribution, although the phase of the periodic interferometer error may change, resulting in this case in a more significant uncertainty source (described more in the experimental section).

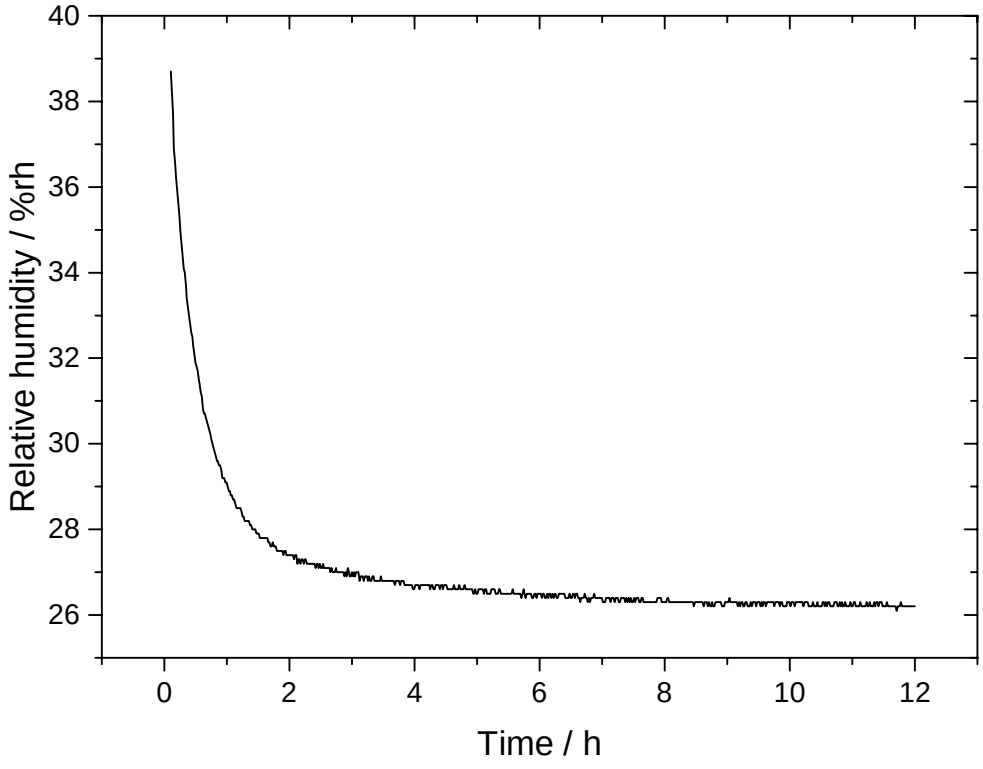

Figure 3. A 12-hour run of circulating air only via the silica gel dryer and measuring AFM enclosure humidity.

3. Force-distance adhesion measurements

In order to study the interaction between AFM probe and sample in different humidities, force-distance, or force-displacement measurements were conducted. First a test result using a palladium coated wide-apex probe with a compliant, i.e. flexible, cantilever is shown. Then two experiments with sharper silicon tips with higher stiffness are then presented. The relatively sharp silicon probe and the silicon sample were selected based on availability of suitable materials that could be easily modelled with the atomistic molecular dynamics simulation. In all the experiments, the sample vertical movement speed was between 1 nm/s and 20 nm/s. The sampling rates used for the presented data were approximately 10 Hz (and each data point is an average of data collected during an averaging window of approximately 20 ms). The humidification chamber of the humidity controller was slightly heated with a thermoelectric element to help attaining the highest humidities used. The traceability of the sample position measurement comes directly from the calibrated laser wavelength used in the interferometers [22].

3.1 Platinum coated probe

In this first test, a platinum coated wider probe (APPNANO ANSCM-PC) with a nominal tip apex radius of 30 nm and stiffness of 0.1 N/m was used to touch a silicon sample. In this case, tip detaching results in the familiar discrete jump out of contact often seen with low-stiffness probes, when the vertical force gradient of probe-sample force is steeper than the deflection force gradient due to the force constant of the probe.
In figure 4, the amplitude of this jump in cantilever deflection has been plotted against time, with the relative humidity measured with the primary humidity sensor. The inset graph shows the observed form and hysteresis of the pull-off jump amplitude plotted against relative humidity instead of time. With low-stiffness uncoated silicon probes the maximum force was much less reproducible, changing erratically and randomly (results not shown).

The maximum pull-off force increases with increasing humidity, and then decreases with decreasing humidity, but does not return to the original level like the humidity does. This is possibly due to tip wear during experiment. Our implementation of the thermal noise method [27, 28] used for calibrating the force constant of the cantilever has not been verified with this low cantilever stiffness, so the force scale is not absolute.

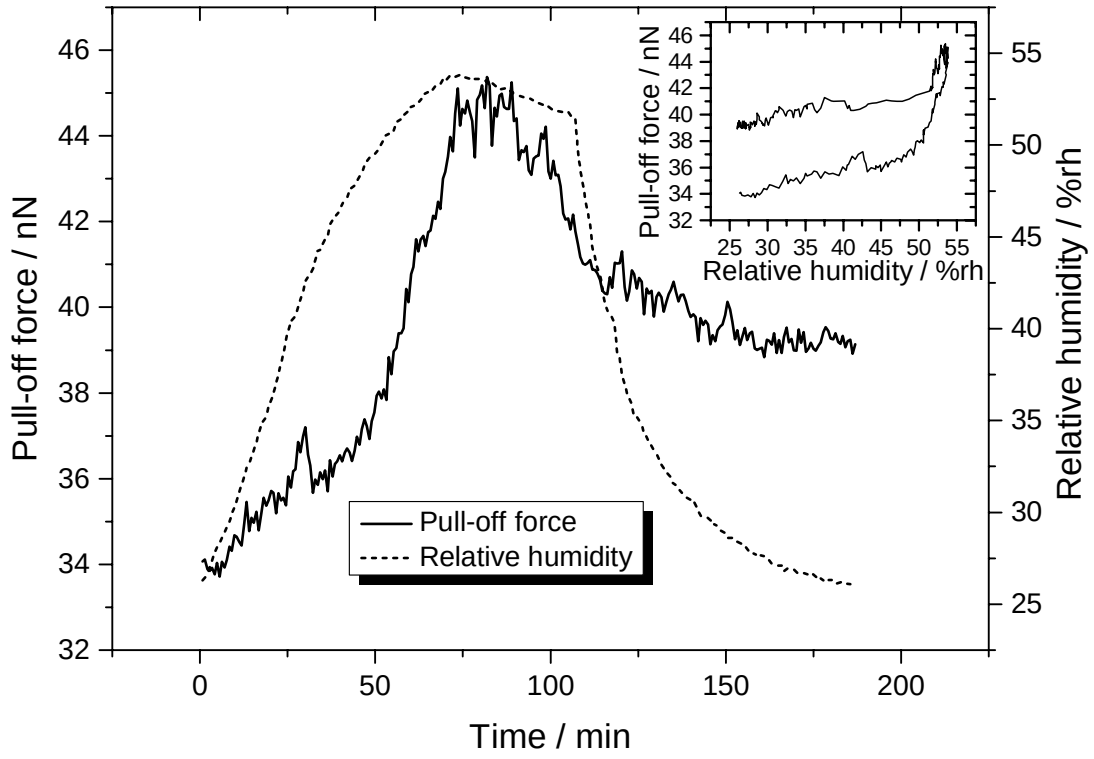

Figure 4. The maximum pull-off force of the platinum coated tip from silicon sample, and relative humidity, during repeated approach-retract adhesion measurements, shown against experiment duration time axis. The inset shows the pull-off force plotted against relative humidity.

1.2 Silicon probe and sample

In these experiments PPP-FMR mid-stiffness probes from Nanosensors, with < 7 nm nominal apex curvature radius, were used in the AFM head for repeatedly touching the underside of another uncoated silicon probe "chip". The AFM chip used as sample was PPP-FMR in experiment A and PPP-NCHR in experiment B. The calibration of tip deflection scale of the AFM photodetector was done via pushing the probe against the silicon sample, and measuring simultaneously the sample stage vertical movement with the vertical (Z) laser interferometer of the IT-MAFM, and the tip deflection "A-B"-signal from the position sensitive photodetector (PSPD) - i.e. similarly to the adhesion measurement but with higher maximum contact force, and by assuming the tip apex and sample as infinitely stiff in this force scale compared to the cantilever stiffness.

After PSPD calibration, in both experiments, the force constant of the cantilever used was measured with the thermal noise method [27, 28] as $k_A = 1.0$ N/m for the PPP-FMR probe used in experiment A and $k_B = 1.1$ N/m for the PPP-FMR probe used in experiment B. Cantilevers of similar order of stiffness were also measured at the Physikalisch-Technische Bundesanstalt, Germany, using a precision compensation balance [29, 30], and the agreement with our implementation of the thermal method for those cantilevers was within 10 %. This is assumed to be the dominating uncertainty component in the presented force measurements.

The experiment was conducted so that first, after aligning the sample below the probe, the AFM enclosurewas steered to 25 %rh, and then the probe was repeatedly approached to and retracted from the sample by moving the sample stage vertically. During the repeated vertical scanning the humidity was first increased to slightly over 50 %rh and then reduced back close to 25 %rh. The range of scanning was kept such that the probe cantilever will slightly touch the sample, and thus bend upwards, in the highest sample position. Temperature near the AFM head was approximately 22 °C in the measurements in experiment A and 23 °C - 24 °C in experiment B. Each approach-retract cycle was done during approximately 2 minutes, and the whole experiment, starting from initial drying, then gradual humidification and dehumidification, took approximately 4 hours. In these experiments the sample was scanned fully vertically instead of scanning orthogonally to the AFM cantilever plane. The speed of the sample vertical movement was less than 10 nm/s, and the tip-sample contact time of several seconds before retraction should be long enough for the liquid bridge to stabilize [6]. The velocity of the tip apex relative to sample was more variable due to the variable bending of the probe cantilever by the interaction forces, especially during snap-in and pull-off type events. In addition to handling with tweezers, the previously unused PPP-FMR probes were not treated or cleaned in any way after removing them from their package, which can possibly affect their properties, if e.g. the Gel-Pak packaging deposits some oil on the probes [31]. The PPP-NCHR probe used as a target sample in experiment B was a steel plate mounted version sold in a plastic packaging box.

Figure 5 shows examples of the force-displacement (f-d) curves when humidity is first increased and then decreased, for experiments A and B. In the tip-sample distance, the tip movement due to cantilever deflection has been subtracted from the interferometrically measured vertical sample position. The graphs have been shifted to match vertical and horizontal parts of curves, to reduce the effect of drifts. In experiment B a drift compensation has also been done on the position axis scale. The drift was estimated from successive scans comparing the observed sample surface position drift in the interferometric coordinates. Stage capacitive sensors were not drifting relative to interfereometers, but the sample surface observed by the AFM head PSPD and Z interferometer was hundreds of nanometres higher in higher humidities, probably due to some mechanical response in e.g. the AFM head to the air humidification and dehumidification in both experiments. Humidities are bit lower on average in experiment B since the instrument was running approximately 1.5 °C warmer due to difference in electrical configuration (AFM head and camera stepper motor brakes were left open, although steppers were not used during measurement. The stepper motor brakes, situated above the AFM head, have an electric current flowing in the solenoid coils when left open. This heats the air circulated in the system, and also slightly warms the AFM head and sample by the heat conducted downwards via the (Invar) steel structural elements of the instrument). The higher probe stiffness combined with smaller interaction force, compared to the platinum coated tip test, usually makes it possible to continuously lift the probe apex relative to the sample, instead of just jumping out of contact, especially in experiment A.

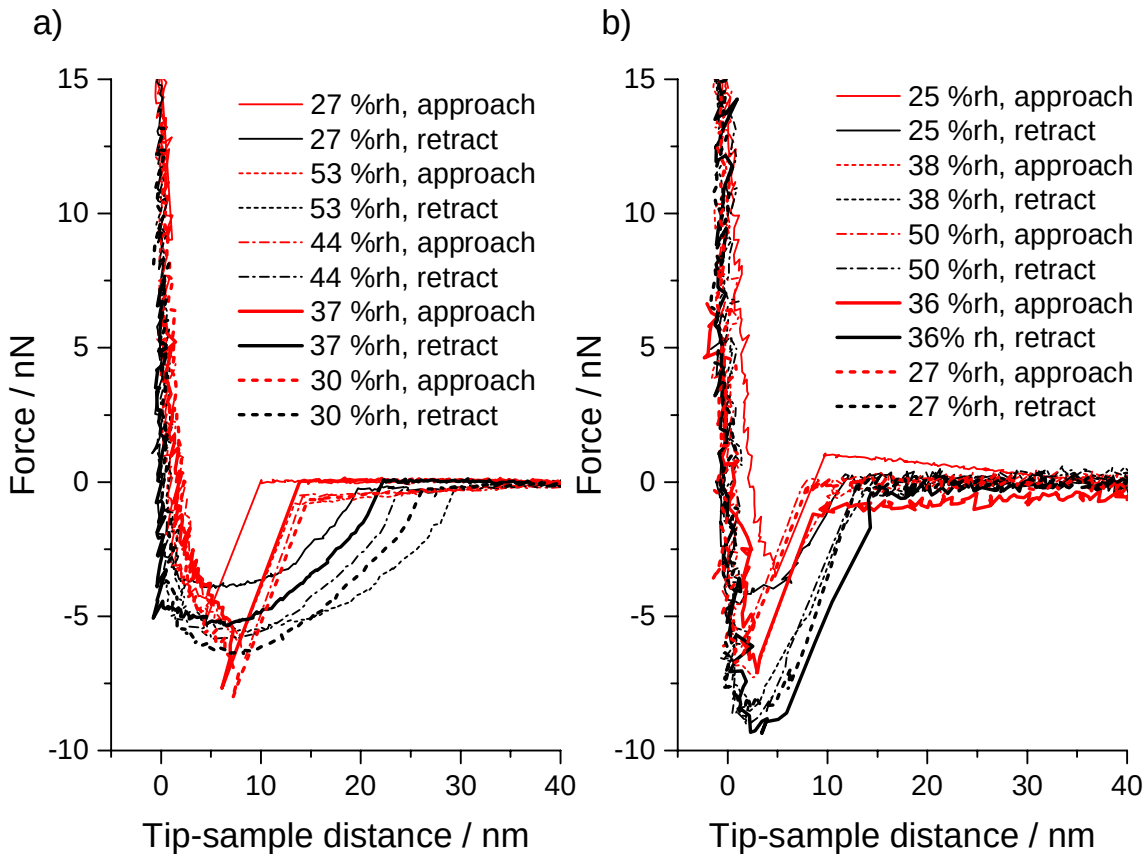

Figure 5. Examples of f-d curves measured a) in experiment A and b) in experiment B. Red/gray indicates approach (loading) and black retraction (unloading) of probe from sample, respectively. The legend indicates the measurements' chronological order, starting from top, first increasing and then decreasing in humidity.

The results of experiments A and B should be ideally similar in all aspects, but clearly there are quite large differences in these two experiments. The peak forces are of similar order, on average somewhat higher in experiment B. During the experiments, forces grow stronger probably due to tip wear. One of the most important differences is that in experiment A the retraction distance needed for the interaction force to "vanish", the break-free distance, is on average twice the length seen in experiment B. Also, in experiment A the variation of this distance is larger, and the variation is not fully systematic with humidity or time. In experiment B the repeatability between consecutive curves in the data was better. Also the stronger peak force in snap-in compared to retraction seen in experiment A is absent in experiment B.

Differences between measurements A and B include, in addition to different probe chip as target and slightly differing temperatures, the fact that different computer program and electronics were used to drive the AFM Z piezo, although recording of PSPD and interferometers was done with the same system in both experiments.

The periodic nonlinearity of the Z laser interferometer was not corrected by measuring a periodic correction in this experiment partly because of the changing ambient conditions in the enclosure. In this measurement's short length scale, this causes an additional uncertainty of mainly Z scale amplification coefficient, of approximately 5% with the instrument.

4. Atomistic molecular dynamics simulation

Models of various complexity exist to predict the size and shape of the meniscus forming between two objects of a given geometry and material, at given relative humidity [7, 9]. While such simple continuum models usually work well for length scales above tens or hundreds of nanometres, they do not take into account the atomistic details of the interface region and the water molecules covering the surfaces and give no information about the dynamics of meniscus formation or rupture, and may not be valid down to nanometre length scales. We have therefore chosen to compare our experimental results from the humidity-controlled AFM measurements to atomistic simulations of a model system, described below.

4.1 Simulation setup

The silicon tip and sample surfaces, as used in experiment, are covered in several nanometres of a native oxide layer (SiO_2), which in turn reacts with water in humid air to form silanol groups (Si-OH). The possibility to form hydrogen bonds between the surface silanol groups and water molecules present in humid air are the reason for the hydrophilic property of this material. We have therefore chosen to model both tip and surface from silicon dioxide, with full silanol coverage at the surfaces. The AFM tip apex is modelled as the lower part of a sphere of radius 5 nm and height 3 nm. In order to simulate different humidity conditions, we have covered the surfaces with water layers of appropriate thickness, determined by IR spectroscopy experiments. The variations between the experimental values for the thickness of the water layer on silicon dioxide in literature are small [32-34], and we have chosen heights of h = 0.6, 0.8, and 1.0 nm to represent 20, 40 and 60 %rh, respectively. The silica slab measured approximately 17.5 nm × 17.5 nm × 1.0 nm, and the height of the simulation box was 20 nm, which was deemed large enough to avoid spurious interactions through periodic boundary conditions. Depending on the humidity, the systems (illustrated in figure 6) consisted of 55959, 66669, or 77478 atoms. The ClayFF force field [35] was used to describe SiO_2/SiOH/water interactions, and SPC/Fw [36] for water-water interactions, which reproduce the properties of the silica/water interface [37, 38], and bulk water [36, 39] reasonably well. The tip approach and retraction was simulated with steered MD, using the LAMMPS code [40] with the PLUMED plug-in [41]. The tip was initially placed at d = 5.5 nm above the surface, and then slowly pulled to d = 1.5 nm and retracted back to d = 7.5 nm, in a moving harmonic spring of force constant k = 500 eV/Å along z, perpendicular to the surface Additional harmonic constraints with a force constant of 100 eV/Å along x and y were placed on Si atoms in the tip to avoid lateral drift. Similarly, harmonic constraints along x, y, and z were placed on Si atoms in the slab, to immobilize it with respect to the frame of reference of the simulation box. The rate of pulling was 1 nm/ns, and a Nosé-Hoover thermostat was used to maintain a temperature of 300 K in the system.

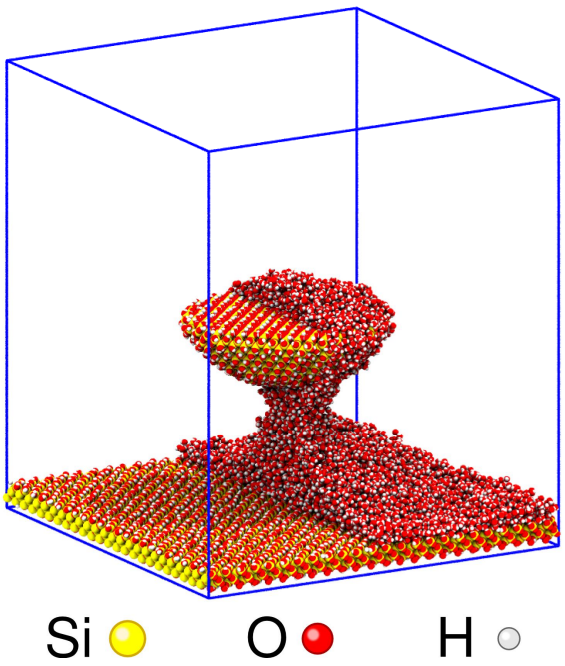

Figure 6. Simulation setup: A snapshot of the atomistic simulation showing the simulation box (blue lines) containing the silicon dioxide slab at the bottom, the spherical AFM tip apex, and water coverage corresponding to 40 %rh. Only the water molecules in one half of the simulation box are shown, to reveal the tip and sample surfaces and emphasize the atomic scale of the meniscus and surface water layers. Silicon atoms are colored in yellow, oxygen atoms in red, and hydrogen atoms in white (color online).

4.2 Simulation results

The force-distance curves obtained along approach and retraction of the tip at 20 %rh, 40 %rh, and 60 %rh are presented in figure 7. The general shape of the curves is similar for all three humidity values considered: initially, while the tip is far away (positions 1), the forces are close to zero. Upon approach, the water layers covering tip and surface are brought closer together, until a thermal fluctuation of a water molecule at the liquid/air interface leads to the formation of the meniscus (positions 2). The formation of the meniscus coincides with the appearance of attractive capillary forces between tip and sample, which increase with decreasing tip-sample distance, and growth of the meniscus, until the closest tip approach in the simulation is reached, and the tip is subsequently retracted (positions 3). When the tip reaches the distance at which the meniscus was initially formed upon approach, a much larger meniscus is now observed (positions 4). The tip needs to be retracted several nanometres further, before the rupture of the meniscus can be observed, and the force vanishes again (positions 5). The meniscus breaks when the force exerted on the neck breaks the few remaining hydrogen bonds. After the rupture of the meniscus, the forces return to zero and the water layers on the tip and surface re-equilibrate until the final positions in the simulations are reached (positions 6).
As expected, the meniscus forms and breaks at larger distances, when the humidity is higher, and more water molecules are present in the system. We also observe that the difference between the tip-surface distance where it forms (d_{on}) and ruptures (d_{off}) increases with humidity: the meniscus can be extended by 2.5 nm, 3.0 nm, and 3.6 nm at 20 %rh, 40 %rh, and 60 %rh, respectively. We also observe an increase in the magnitude of the attractive capillary forces at similar tip-sample distances with increasing humidity, however the difference in maximum force observed at 20 %rh and 60 %rh is only around 10 %.

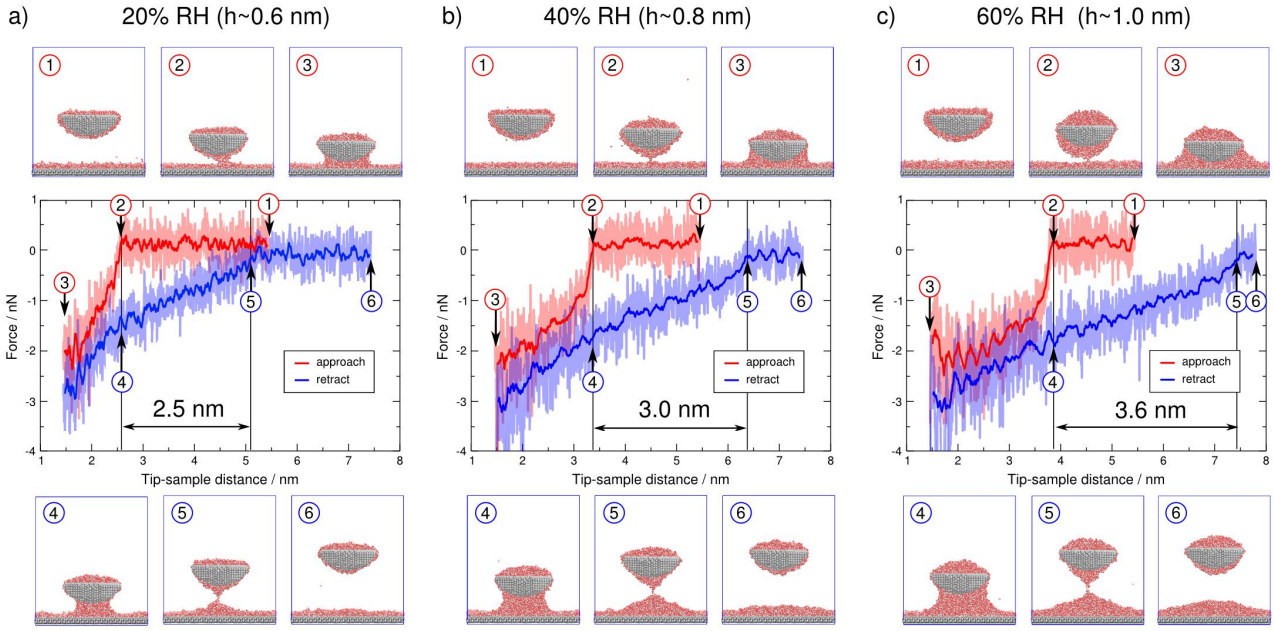

Figure 7. Force-distance curves from simulation at a) 20 %rh, b) 40 %rh and c) 60 %rh. Simulation snapshots along approach (red) and retraction (blue) curves illustrate the starting configuration (1), the formation of the meniscus (2), the closest tip approach (3), the meniscus when the tip is retracted back to the same distance where it was originally formed (4), the rupture of the meniscus (5), and the final configuration (6). The difference in tip-sample distance between positions (2) and (5) marks the maximum elongation of the meniscus at that RH value.

5. Discussion

In the measurements of experiment A with a silicon probe and sample, with both increasing and decreasing humidity, the highest humidity provides the longest break-free length, and driest or second-driest provides the shortest. The repeatability of the adhesion measurements with the silicon probe could be possibly enhanced by averaging several f-d curves and by ensuring that no contaminants interfere with the measurement, or on the other hand, by limiting tip wear during repeated contacting. In experiment A the break-free lengths seem not to be fully ordered according to humidity. One could argue that the average increase in break-free length in figure 5a is a few nanometres, almost in accordance with the simulation, or on the other hand, that the driest humidity curve is an anomaly due to contamination on the sample or tip and the meniscus elongation is larger. The measured break-free distance in experiment A is also quite long compared to other studies [3].

In experiment B the observed shape of the force curve and break-free distance are in better accordance with the simulation results presented, and the repeatability between successive f-d measurements was better than in experiment A, where in the humidification phase we also measured some curves with erratic shapes not shown in the results. In experiment B however, the gradients of the interaction forces are close the regimen where a sudden jump off contact, or pull-off, happens, making the number of data points on the rising part of the unloading, or retraction, curve so low that analysis of the meniscus elongation is more difficult.

In experiment B the break-free length observed in the second-last curve (36 %rh) after the maximum humidity appears to be the longest, but analysed the same way as the simulation results, i.e. as the difference

between meniscus formation and breaking, this difference becomes negligible. We also note that the interaction strengths as e.g. pull-off forces can present several local maxima or parabolic shapes as function of relative humidity [5]. The larger variation in pull-off force with hydrophilic probe and silicon sample when relative humidity is changed, e.g. as reported by He et al. [42], occurred close to 50 rh%, which is at the end of the humidity range used here. Also, it is possible that the Gel-Pak storage has rendered the AFM tips more hydrophobic.

The differences in results between experiments A and B are so far not fully understood. Possible contributions include different contamination of tip and sample as well as stage vibration. On average the interaction force seems to be increasing during experiments due to tip wear in the test with the platinum coated tip as well as in both the experiments A and B with uncoated silicon probes. More work is needed to reduce the apparent tip wear during experiments. In the future, a measurement of the tip apex size, using e.g. a surface with suitable nanoroughness imaged before and after an experiment, could help in determining the total amount of tip wear and the tip size. Also using a gentler sample approach and smallest possible maximum force could reduce the tip wear. Furthermore, it would be beneficial to study the need for and effect of cleaning treatments for probes before measurements.

The atomistic simulations of a model system of AFM tip and sample of similar dimensions in humid air agree in several aspects with our experimental results. We observe the two distinct curves along approach and retraction with a clear signature of formation and breaking of a meniscus between tip and sample. The capillary forces due to the meniscus are of the same order of magnitude as in experiment (several nanonewtons), and increase slightly with relative humidity. The maximum elongation of the meniscus (the difference between the distance where the meniscus forms and breaks) also increases with humidity. The measurement results presented are somewhat inconclusive on this elongation, and there are uncertainty factors in both in the simulation and experiment related to meniscus elongation. The factors include trivial differences that may exist between simulated system and experiment (the tip radii are most likely different, and the shape of the apex is probably not perfectly spherical), but there are also two limitations in the computational method employed: first, our simulations were carried out at constant number of particles (NVT ensemble), which means that diffusion of water molecules from the liquid layers originally present on tip and sample was the only source of water molecules for growing the meniscus. In reality, water at the interface is in equilibrium with the gas phase, and water molecule depletion in the liquid layers can be compensated through condensation, sustaining the growth and postponing the rupture of the meniscus upon tip retraction. In addition, the pulling rate of 1 m/s in the simulation is many orders of magnitude faster than in experiment. In fact, the forces on the tip during approach, before the formation of the meniscus, are on average slightly repulsive – an indication that the pulling speed is too large. This also means that upon retraction of the tip, the meniscus may be stretched faster than water molecules can diffuse into it from the surfaces, which leads to a preliminary rupture of the meniscus. In a future study, these issues could be addressed by carrying out simulations with slower pulling speeds and in the grand canonical ensemble, where the number of water molecules is adjusted to keep the chemical potential constant with respect to the chosen value of the relative humidity. Such methods are computationally more expensive, and have in the present context only been applied to simpler lattice-gas systems [8], or atomistic systems at smaller scales [43].

6. Conclusion

A humidity control system for the metrology AFM at VTT MIKES was designed and implemented. The developed instrument permits humidity controlled metrology AFM measurements with direct laser

interferometric sample position measurement. Adhesion measurements with platinum coated and uncoated silicon probes on silicon samples were performed, and an atomistic molecular dynamics simulation was set up, modelling an experiment similar to the measurements with the uncoated silicon probe. The test with a wider platinum coated probe demonstrated the measurement of effects of relative humidity on the maximum pull-off force with the humidity controlled metrology AFM.

In the experiments with uncoated silicon probes the use of stiffer, relatively sharp silicon probes, along with the molecular dynamics simulation, provides a more detailed view on the evolution of the water meniscus compared to studies with soft cantilevers that show discrete pull-off jumps, and compared to modelling capillary processes based on continuum theories. We observe similar behaviours in the experiments with uncoated silicon probes on silicon samples in the 25 – 53 %rh range, and the atomistic simulations at 20, 40, and 60 %rh. Maximum attractive forces were of similar order of magnitude – approximately 3 nN in the simulations and 2-4 nN in the beginning of repeated f-d measurements, subsequently increasing to 7-9 nN, probably mostly due to tip wear. The atomistic simulations show hysteresis similar to experiments in force-distance curves between approach and retraction, and enable us to 'see' the details of meniscus formation and rupture. The measurement results further agree with the simulation in that the maximum capillary force is not strongly affected by the relative humidity, whereas the maximum length of the water bridge between sample and tip before rupture upon tip retraction may depend more strongly on the relative humidity, in the range of relative humidity studied. So far however, the variability in the presented measurements, the unknown true tip apex geometry, as well as the limitations of the simulation method, make a quantitative comparison of the meniscus elongation results difficult.

Acknowledgments

This work has been supported by the European Metrology Research Program (EMRP) project MechProNO and Researcher Excellence Grant EMRP NEW05-REG2, and by the Australian Research Council Discovery Programme (DP 140101776 and FT 130100463). The EMRP is jointly funded by the EMRP participating countries within EURAMET and the European Union. We acknowledge use of the computational resources provided by the Australian Government and the Government of Western Australia through the Pawsey Supercomputing Centre under the National Computational Merit Allocation Scheme.

References

[1] Chen L, Gu X, Fasolka M J, Martin J W and Nguyen T 2009 Effects of Humidity and Sample Surface Free Energy on AFM Probe-Sample Interactions and Lateral Force Microscopy Image Contrast *Langmuir* **25** 3494-3503 doi:10.1021/la8037928

[2] Verdaguer A, Santos S, Sauthier G, Segura J J, Chiesa M and Fraxedas J 2012 Water-mediated height artifacts in dynamic atomic force microscopy *Phys. Chem. Chem. Phys.* **14** 16080-16087 doi:10.1039/c2cp43031b

[3] Binggeli M and Mate CM 1994 Influence of capillary condensation of water on nanotribology studied by force microscopy *Appl. Phys. Lett.* **65** 415 doi:10.1063/1.113020

[4] Stukalov O, Murray C A, Jacina A and Dutcher J R 2006 Relative humidity control for atomic force microscopes *Rev. Sci. Instrum.***77** 033704 doi:10.1063/1.2182625 (and references therein)

[5] Jones R, Pollock H M, Cleaver J A S and Hodges C S 2002 Adhesion Forces between Glass and Silicon Surfaces in Air Studied by AFM: Effects of Relative Humidity, Particle Size, Roughness, and Surface Treatment *Langmuir* **18** 8045-8055 doi:10.1021/la0259196

[6] Wei Z and Zhao Y-P 2007 Growth of liquid bridge in AFM *J. Phys. D: Appl. Phys*. **40** 4368–75 doi:10.1088/0022-3727/40/14/036

[7] Pakarinen O H, Foster A S, Paajanen M, Kalinainen T, Katainen J, Makkonen I, Lahtinen J and Nieminen R M 2005 Towards an accurate description of the capillary force in nanoparticle-surface interactions. *Modelling Simul. Mater. Sci. Eng.* **13**, 1175–1186. doi:10.1088/0965-0393/13/7/012
[8] Jang J and Schatz G C 2010 Lattice Gas Monte Carlo Simulation of Capillary Forces in Atomic Force Microscopy *J. Adhes. Sci. Technol.* **24** 2429–2451 doi:10.1163/016942410X508172
[9] Butt H-J and Kappl M 2009 Normal capillary forces *Adv. Colloid Interface Sci.*, **146** 48–60 doi:10.1016/j.cis.2008.10.002
[10] Guillot B 2002 A reappraisal of what we have learnt during three decades of computer simulations on water *J. Mol. Liqu.* **101** 219–260 doi:10.1016/S0167-7322(02)00094-6
[11] Sedlmeier F, Janecek J, Sendner C, Bocquet L, Netz R R and Horinek D 2008 Water at polar and nonpolar solid walls (Review) *Biointerphases* **3** FC23 doi:10.1116/1.2999559
[12] Limmer, D. T., Willard, A. P., Madden, P., & Chandler, D. (2013). Hydration of metal surfaces can be dynamically heterogeneous and hydrophobic *Proc. Nat. Acad. Sci.* **110** 4200–4205 doi:0.1073/pnas.1301596110
[13] Vila Verde A, Bolhuis P G and Campen R K 2012 Statics and Dynamics of Free and Hydrogen-Bonded OH Groups at the Air/Water Interface *J. Phys. Chem. B* **116** 9467–9481 doi:10.1021/jp304151e
[14] Rahaman A, Grassian V H and Margulis C J 2008 Dynamics of Water Adsorption onto a Calcite Surface as a Function of Relative Humidity *J. Phys. Chem. C* **112** 2109–2115 doi:10.1021/jp077594d
[15] Wensink E J W, Hoffmann A C, Apol M E F and Berendsen H J C 2000 Properties of Adsorbed Water Layers and the Effect of Adsorbed Layers on Interparticle Forces by Liquid Bridging *Langmuir*, **16** 7392–7400 doi:10.1021/la000009e
[16] Li T-D, Gao J, Szoszkiewicz R, Landman U and Riedo E 2007 Structured and viscous water in subnanometer gaps *Phys. Rev. B* **75** 115415 doi:10.1103/PhysRevB.75.115415
[17] Mittal J and Hummer G 2010 Interfacial thermodynamics of confined water near molecularly rough surfaces *Faraday Discuss.* **146** 341-352 doi:10.1039/b925913a
[18] Tang C Y and Zhang L C 2004 A molecular dynamics analysis of the mechanical effect of water on the deformation of silicon monocrystals subjected to nano-indentation *Nanotechnology* **16** 15–20 doi:10.1088/0957-4484/16/1/004
[19] Watkins M and Shluger A 2010 Mechanism of Contrast Formation in Atomic Force Microscopy in Water *Phys. Rev. Lett.* **105** 196101 doi:10.1103/PhysRevLett.105.196101
[20] Fukuma T, Reischl B, Kobayashi N, Spijker P, Canova F F, Miyazawa K and Foster A S 2015 Mechanism of atomic force microscopy imaging of three-dimensional hydration structures at a solid-liquid interface *Phys. Rev. B* **92** 155412 doi:10.1103/PhysRevB.92.155412
[21] Traceable measurement of mechanical properties of nano-objects, [Online], Available: www.ptb.de/emrp/mechprono-home.html, accessed Feb 26, 2016
[22] Korpelainen V, Seppä J and Lassila A 2010 Design and Characterization of MIKES Metrological Atomic Force Microscope *Precis. Eng.* **34** 735-744 doi:10.1016/j.precisioneng.2010.04.002
[23] Lassila A, Kari M, Koivula H, Koivula U, Kortström J, Leinonen E, Manninen J, Manssila J, Mansten T, Meriläinen T, Muttilainen J, Nissilä J, Nyblom R, Riski K, Sarilo J and Isotalo H 2011 Design and performance of an advanced metrology building for MIKES, *Measurement* **44** 399–425 doi:10.1016/j.measurement.2010.10.013
[24] Sairanen H, Heinonen M and Högström R 2015 Validation of a calibration set-up for radiosondes to fulfil GRUAN requirements *Meas. Sci. Technol.* **26** 105901 doi:10.1088/0957-0233/26/10/105901
[25] Bönsch G and Potulski E 1998 Measurement of the refractive index of air and comparison with modified Edlén's formulae *Metrologia* **35** 133-9 doi: 10.1088/0026-1394/35/2/8
[26] Refractive Index of Air Calculator, [Online], Available: http://emtoolbox.nist.gov/Wavelength/Edlen.asp, accessed Aug 22, 2016]
[27] Burnham N A, Chen X, Hodges C S, Matei G A, Thoreson E J, Roberts C J, Davies M C, and Tendler S J B 2003 Comparison of calibration methods for atomic-force microscopy cantilevers *Nanotechnology* **14** 1-6 doi:10.1088/0957-4484/14/1/301
[28] Cook S M, Schäffer T, Chynoweth K, Wigton M, Simmonds R and Lang K 2006 Practical implementation of dynamic methods for measuring atomic force microscope cantilever spring constants *Nanotechnology* **17** 2135 doi:10.1088/0957-4484/17/9/010
[29] Behrens I, Herold B, Doering L and Peiner E 2003 Piezoresistive cantilever as portable micro force calibration standard *J. Micromechanics Microengineering* **13** S171–S177

[30] Kim M-S, Pratt J R, Brand U, and Jones C W 2012 Report on the first international comparison of small force facilities: a pilot study at the micronewton level *Metrologia* **49** 70-81 doi:10.1088/0026-1394/49/1/011
[31] Lo Y-S, Huefner N D, Chan W S, Dryden P, Hagenhoff B and Beebe T P Jr. 1999 Organic and Inorganic Contamination on Commercial AFM Cantilevers *Langmuir* **15** 6522–6526 doi:10.1021/la990371x
[32] Asay D B and Kim S H 2005 Evolution of the Adsorbed Water Layer Structure on Silicon Oxide at Room Temperature *J. Phys. Chem.* B **109** 16760–16763 doi:10.1021/jp053042o
[33] Verdaguer A, Weis C, Oncins G, Ketteler G, Bluhm H, and Salmeron M 2007 Growth and Structure of Water on SiO_2 Films on Si Investigated by Kelvin Probe Microscopy and in Situ X-ray Spectroscopies *Langmuir* **23** 9699–9703 doi:10.1021/la700893w
[34] Takahagi T, Sakaue H and Shingubara S 2001 Adsorbed water on a silicon wafer surface exposed to atmosphere *Japan. J. Appl. Phys.* **40** 6198–201 doi:10.1143/JJAP.40.6198
[35] Cygan R T, Liang J-J and Kalinichev A G 2004 Molecular Models of Hydroxide, Oxyhydroxide, and Clay Phases and the Development of a General Force Field *J. Phys. Chem.* B **108** 1255–1266 doi:10.1021/jp0363287
[36] Wu Y, Tepper, H L and Voth G A 2006 Flexible simple point-charge water model with improved liquid-state properties *J. Chem. Phys.* **124** 024503 doi:10.1063/1.2136877
[37] Leroch S and Wendland M 2012 Simulation of Forces between Humid Amorphous Silica Surfaces: A Comparison of Empirical Atomistic Force Fields *J. Phys. Chem.* C **116** 26247–61 doi:10.1021/jp302428b
[38] Skelton A A, Wesolowski D J and Cummings P T 2011 Investigating the Quartz (10-10)/Water Interface using Classical and Ab Initio Molecular Dynamics *Langmuir* **27** 8700–8709 doi:10.1021/la2005826
[39] Vega C and de Miguel E 2007 Surface tension of the most popular models of water by using the test-area simulation method *J. Chem. Phys.* **126** 154707 doi:10.1063/1.2715577
[40] Plimpton S 1995 Fast Parallel Algorithms for Short-Range Molecular Dynamics *J. Comp. Phys*. **117** 1-19 doi:10.1006/jcph.1995.1039, http://lammps.sandia.gov
[41] Tribello G A, Bonomi M, Branduardi D, Camilloni C and Bussi G 2014 PLUMED 2: New feathers for an old bird. *Comput. Phys. Comm.* **185** 604-13 doi:10.1016/j.cpc.2013.09.018
[42] He M, Szuchmacher Blum A, Aston D E, Buenviaje C, Overney R M and Luginbühl R 2001 Critical phenomena of water bridges in nanoasperity contacts *J. Chem. Phys.* **114** 1355-1360 doi:10.1063/1.1331298
[43] Kim H, Smit B, and Jang J 2012 Monte Carlo Study on the Water Meniscus Condensation and Capillary Force in Atomic Force Microscopy *J. Phys. Chem.* C **116** 21923–21931 doi:10.1021/jp307811q